INTERNATIONAL JOURNAL FOR NUMERICAL METHODS IN FLUIDS
Int. J. Numer. Meth. Fluids 2002; **38**:567–588 (DOI: 10.1002/fld.235)

An unconditionally stable, explicit Godunov scheme for systems of conservation laws

Vincent Guinot[*,†]

*International Institute for Infrastructural Hydraulics and Environmental Engineering—IHE,
Westvest 7, P.O. Box 3015, 2601 DA Delft, The Netherlands*

SUMMARY

Common explicit, Godunov-type schemes are subject to a stability constraint. The time-line interpolation technique allows this constraint to be eliminated without having to make the scheme implicit or to linearize the equations. For 2×2 systems of conservation laws, a system of non-linear equations has to be solved in the general case to determine the left and right states of the Riemann problems at the cell interfaces. However, if one cell in the domain is wide enough for the Courant number to be locally lower than unity, it is not necessary to solve a system anymore and the values at the next time step can be computed directly. The method is detailed for linear and non-linear scalar advection, as well as for 2×2 systems of hyperbolic conservation laws. It is illustrated by an application to a simplified model for two-phase flow in pipes, which is described using a 2×2 system of non-linear hyperbolic equations. Copyright © 2002 John Wiley & Sons, Ltd.

KEY WORDS: Godunov schemes; explicit; unconditionally stable

1. INTRODUCTION

Godunov-type schemes are a very powerful technique to handle discontinuous flows arising from the non-linear character of hyperbolic Partial Differential Equations (PDEs). Industrial applications of these schemes have to cope with irregular geometries and, even for one-dimensional problems, it may be necessary to refine the computational grid locally. Owing to the classical Courant–Friedrichs–Lewy (CFL) stability constraint associated with classical explicit schemes, local mesh refinement leads to time step reduction. This yields an increase of the computational effort, as well as a degradation of scheme performance in the regions of the computational domain where mesh refinement is not needed. The classical answer of model developers consists of developing implicit schemes. A number of implicit Godunov-types schemes have been proposed [1–4]. Although solving the problem of stability—at least in a linear context (see Reference [2] about problems arising from non-linearity)—these schemes

[*] Correspondence to: V. G. Guinot, Department of Hydrology & Hydroinformation, International Institute for Infrastructural Hydraulics and Environmental Engineering, IHE, Westvest 7, P.O. Box 3015, 2601 DA Delft, The Netherlands.

[†] E-mail: vgt@ihe.nl

Received May 2000
Revised 20 June 2001

need systems of equations to be inverted, making the computational procedure expensive. Moreover, some of them introduce a linearization of the PDEs to be solved. Attempts to increase the accuracy in time lead to bigger systems (see Reference [1]). On the other hand, explicit schemes have been designed to handle large time steps and extended to multiple dimensions [5–7]. These methods consider the full extent of the domain of dependence of the solution in space and therefore lead to variable stencils covering several cells in space when needed by the time step. In this approach, a particular procedure has to be followed to take into account the possible presence of several shocks and rarefaction waves within the domain of dependence of the solution, since these waves may interact or merge within a single time step. This leads to increased computational time. In References [6] and [7], it is suggested that an approximate Riemann solver like that designed by Roe [8] could lead to proper linearization of the conservation laws to be solved and to simplify the handling of wave interactions.

The proposed approach allows CFL values higher than unity to be used, without having to make the scheme implicit. It is not necessary either to have recourse to variable stencils in space, since the scheme uses information contained in the characteristic lines that cross neighbouring interfaces rather than the value of the variable at the next time level. A somewhat similar procedure, called time-line interpolation, was used in combination with the Method of Characteristics in the field of hydraulics in the 1970s [9]. In the proposed approach, a system of equations still has to be solved, unless there is one mesh within the computational domain where the Courant number is smaller than unity. Moreover, in contrast to the above-mentioned approach [5–7], the proposed method propagates directly the results of each wave interaction from one wave to the next, which makes the treatment of such interactions much easier and faster. Eventually, no linearization of the conservation laws is needed for the treatment of wave interactions.

Section 2 describes the principle and implementation of the proposed method for linear and non-linear scalar advection. Section 3 focuses on its application to the 2 × 2 system of hyperbolic conservation laws that describe two-phase flows in pipes. Section 4 provides computational examples for the three types of equations above and Section 5 is devoted to remarks and conclusions. Appendix A is devoted to the stability and consistency analysis of the proposed solution for linear advection problems with constant coefficients. Appendix B presents a method to solve the generalized Riemann problem.

2. SCALAR ADVECTION

2.1. Linear advection

Consider the Partial Differential Equation (PDE) that describes one-dimensional, linear scalar advection:

$$\frac{\partial \phi}{\partial t} + \frac{\partial F}{\partial x} = 0 \tag{2.1a}$$

$$F = a\phi \tag{2.1b}$$

where ϕ (arbitrary unit) is the advected variable, F (arbitrary unit) is the flux, a (m s^{-1}) is the velocity, x (m) is the space-coordinate, and t (s) is time. Equation (2.1a) can be discretized according to the finite-volume approach:

$$\Phi_j^{n+1} = \Phi_j^n + \frac{\Delta t}{\Delta x_j}(F_{j-1/2}^{n+1/2} - F_{j+1/2}^{n+1/2}) \tag{2.2}$$

where Φ_j^n is the average value of the solution ϕ over cell j at time level n, $F_{j+1/2}^{n+1/2}$ is the average value of the flux at interface $j+1/2$ between cells j and $j+1$ between time levels n and $n+1$, Δt (s) is the time step and Δx_j is the size of cell j. The average of the flux at the interface is given by:

$$F_{j+1/2}^{n+1/2} = \frac{1}{\Delta t}\int_{t^n}^{t^{n+1}} F[\phi(x_{j+1/2}, t)]\,\mathrm{d}t \tag{2.3}$$

Assume that a is positive. The integral in Equation (2.3) can be separated into:

$$F_{j+1/2}^{n+1/2} = \frac{1}{\Delta t}\int_{t^n}^{t_A} F[\phi(x_{j+1/2}, t)]\,\mathrm{d}t + \frac{1}{\Delta t}\int_{t_A}^{t^{n+1}} F[\phi(x_{j+1/2}, t)]\,\mathrm{d}t \tag{2.4}$$

where A denotes the intersection in the (x, t) plane between the characteristic curve issuing from $(j-1/2, n)$ and the line $(x = x_{j+1/2})$ (see Figure 1). t_A is given by:

$$t_A = t^n + \frac{\Delta x_j}{a} \tag{2.5}$$

In Equation (2.4) the integrals are estimated using a technique that will also be used for non-linear advection. The flux function F is computed using the average value of ϕ:

$$\int_{t_1}^{t_2} F[\phi(x_{j+1/2}, t)]\,\mathrm{d}t = (t_2 - t_1)F\left[\frac{1}{t_2 - t_1}\int_{t_1}^{t_2} \phi(x_{j+1/2}, t)\,\mathrm{d}t\right] \quad \text{for all } t_1, t_2 \tag{2.6}$$

Equation (2.4) then becomes:

$$\begin{aligned} F_{j+1/2} &= \frac{1}{Cr_j}F\left[\frac{1}{t_A - t^n}\int_{t^n}^{t_A} \phi(x_{j+1/2}, t)\,\mathrm{d}t\right] \\ &\quad + \left(1 - \frac{1}{Cr_j}\right)F\left[\frac{1}{t^{n+1} - t_A}\int_{t_A}^{t^{n+1}} \phi(x_{j+1/2}, t)\,\mathrm{d}t\right] \end{aligned} \tag{2.7a}$$

$$Cr_j = \frac{a\Delta t}{\Delta x_j} \tag{2.7b}$$

Using the theory of characteristics, it can be shown that the first integral in Equation (2.7a) is equivalent to the average value of ϕ over cell j at time level n. The second integral giving the average value of ϕ in Equation (2.7a) is transformed into that of ϕ over time at interface $j-1/2$ (see Figure 1):

$$F_{j+1/2}^{n+1/2} = \frac{1}{Cr_j}F(\Phi_j^n) + \left(1 - \frac{1}{Cr_j}\right)F\left[\frac{1}{t_{B'} - t_{A'}}\int_{t_{A'}}^{t_{B'}} \phi(x_{j-1/2}, t)\,\mathrm{d}t\right] \tag{2.8}$$

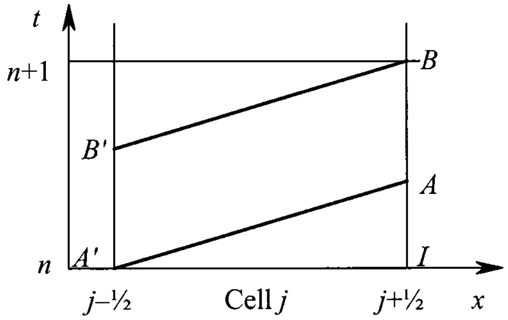

Figure 1. Sketch of the advection problem in the x–t plane.

where A' is point $(j-1/2, n)$ in the $(x-t)$ plane and B' represents the intersection of the characteristic issuing from $(j+1/2, n+1)$ and the line $(x = x_{j-1/2})$. In order to estimate the average value of ϕ over $[A'B']$, the average value of ϕ at the interface $j-1/2$ between t^n and t^{n+1} is used. Equation (2.8) then becomes:

$$F_{j+1/2}^{n+1/2} = \frac{1}{Cr_j} F(\Phi_j^n) + \left(1 - \frac{1}{Cr_j}\right) F(\phi_{j-1/2}^{n+1/2}) \tag{2.9}$$

where $\phi_{j-1/2}^{n+1/2}$ is the average value of ϕ over time between t^n and t^{n+1} at interface $j-1/2$. In the case of linear advection, for which the flux is proportional to ϕ, Equation (2.9) can be rewritten as:

$$F_{j+1/2}^{n+1/2} = \frac{a}{Cr_j} \Phi_j^n + \left(1 - \frac{1}{Cr_j}\right) F_{j-1/2}^{n+1/2} \tag{2.10}$$

Equation (2.10) provides a recurrence relationship that can be used by sweeping the computational domain in the direction of the flow.

2.2. *Non-linear advection*

Consider now the PDE:

$$\frac{\partial \phi}{\partial t} + \frac{\partial F}{\partial x} = 0 \tag{2.11}$$

where the flux function F is an increasing, convex non-linear function of ϕ. The difference with linear advection is that the celerity $\lambda = \mathrm{d}F/\mathrm{d}\phi$ at which the solution propagates is an increasing function of ϕ. This has consequences on the way Cr_j used in Equation (2.9) should be computed.

Consider first the case $\phi_{j-1/2}^{n+1/2} > \Phi_j^n \geqslant 0$ (see Figure 2). Due to the difference between the celerities associated with both states, a shock appears. The speed of this shock is given by:

$$c_s = \frac{F(\phi_{j-1/2}^{n+1/2}) - F(\Phi_j^n)}{\phi_{j-1/2}^{n+1/2} - \Phi_j^n} \tag{2.12}$$

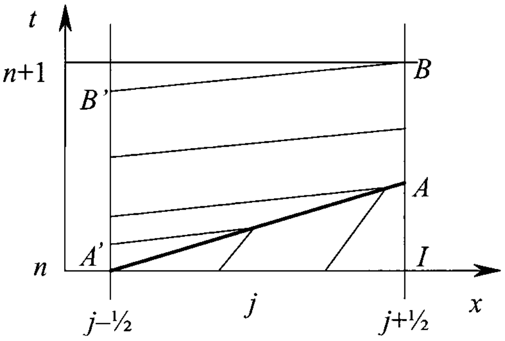

Figure 2. Sketch of a shock moving to the right in the x–t plane. The thin lines show the characteristics on the right and left sides of the shock.

The location of point A is determined by the value of c_s. Therefore, the Courant number Cr_j in Equation (2.10) must be computed using the speed of the shock:

$$Cr_j = \frac{c_s \Delta t}{\Delta x_j} \tag{2.13}$$

Conversely, if $0 \leqslant \phi_{j-1/2}^{n+1/2} < \Phi_j^n$, a rarefaction wave appears. Then, the function $\phi(x_{j+1/2}, t)$ consists of two zones of constant state, connected by a decreasing function of time. In order to save computational time, the rarefaction wave is assimilated to a shock, propagating at the celerity c_s given by Equation (2.12). Equation (2.9) can still be used. Although violating the entropy principle, this approach was found to yield no unrealistic solutions.

Still, Equation (2.13) is valid only when the sign of the wave speed is positive all throughout the computational domain. However, many physical problems involve the interaction between waves, the speeds of which are different. Consider for example the case of the inviscid Burger's equation, that is used as a computational example in Section 4. For this equation, the flux F is given by $F = \phi^2$ and the wave speed is $\lambda = 2\phi$. The following Riemann problem:

$$\phi(x, t=0) = \phi_{j+/2,L}^{n+1/2} > 0 \quad \text{for } x \leqslant x_{j+1/2} \tag{2.14a}$$

$$\phi(x, t=0) = \phi_{j+1/2,R}^{n+1/2} < 0 \quad \text{for } x > x_{j+1/2} \tag{2.14b}$$

is characterized by a positive wave speed on the left-hand side of the initial discontinuity and a negative wave speed on the right-hand side. At later times, a shock appears, the speed of which can be determined by applying Equation (2.12):

$$c_s = (\phi_{j+1/2,L}^{n+1/2} + \phi_{j+1/2,R}^{n+1/2})/2 \tag{2.15}$$

The flux across the interface $j + 1/2$ will be computed correctly provided the left and right states of the Riemann problem are properly characterized. Equation (2.13) can therefore be used only for wave positive wave speeds, i.e. for the characterization of the left states of the Riemann problems. In order to determine the right states of the Riemann problems at the cell interfaces, a sweep must be performed from right to left. If the wave speed in a cell is such that the Courant number in this cell is smaller than unity, the left (or right) state of the Riemann problem is determined as in the standard Godunov method, by taking the average of the variable over the computational cell.

2.3. Enhancement of stability for non-linear laws

The time-line interpolation technique presented above consists merely of substituting part of the spatial extent of the domain of dependence of the solution with its corresponding extent in time (see Figure 3). In the figure, the domain of dependence of $[IB'']$ (interface $j+1/2$ between time levels n and $n+1$) is classically $[IB''] = [IA'] \cup [A'B'']$. The time-line transformation consists of using the characteristics-based equivalence between $[A'B'']$ and $[A'B']$. The condition of existence of a solution to Equations (2.1) or (2.11), i.e. the existence of a domain of dependence that exceeds the size of cell j, is not violated. As shown in Appendix A, the present method is only first-order accurate. However, it is a little less dissipative than the classical implicit formulation. In addition, only two points are needed in each direction of space, which makes easier the implementation of the algorithm for multi-dimensional advection.

Another remark should be made on the calculation of the Courant number for further use in Equation (2.9) in the case of non-linear advection. If the propagation celerity of the shock is underestimated, mass accumulates artificially behind the front and oscillations appear, with the possible consequence of non-linear instability. Such a problem was mentioned by Collins *et al.* in 1992 [2]. It is possible to prevent the appearance of oscillations by overestimating the celerity at which the solution propagates. This approach amounts to increasing the upwind character of the discretization by overestimating the extent of the domain of dependence. This technique is used for the extension to 2×2 systems of conservation laws as described in Section 3.

When the Courant number is lower than unity, the flux can be computed directly using the average of the variable ϕ over the domain of dependence of the characteristic, without having recourse to the time-line interpolation.

2.4. Treatment of sonic points for non-linear advection

Another problem to be addressed is that of the possible presence of sonic points in the case of non-linear advection. A sonic point is encountered during the sweep from left to right when

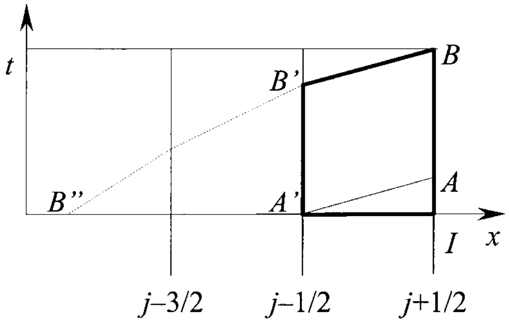

Figure 3. Equivalence of domains of dependence in space and time. Segment $[B''A']$ in space is equivalent to segment $[A'B']$ in time.

the wave speed associated with $\phi_{j-1/2,L}^{n+1/2}$ is negative and that associated with Φ_j^n is positive. In this case, the dependence between $\phi_{j-1/2,L}^{n+1/2}$ and $\phi_{j+1/2,L}^{n+1/2}$ is broken. The best solution found in this case consists of replacing the value of $\phi_{j-1/2,L}^{n+1/2}$ by the value of ϕ that gives a zero wave speed (in the case of the Burgers equation, this value is $\phi = 0$). This substitution guarantees the independence of $\phi_{j+1/2,L}^{n+1/2}$ on the previous values. A similar test must be performed during the sweep from right to left for the right states of the Riemann problem.

2.5. *Algorithm*

The considerations above can be summarized in the form of the following algorithm. This algorithm is valid for linear as well as for non-linear scalar laws.

The first step consists of determining the left states of the Riemann problems. The computational domain is swept from left to right (increasing j), starting from the left-hand boundary. For each interface, the following operations must be made.

(i) For each interface $j+1/2$, determine the wave speeds $\lambda_{j-1/2}^{n+1/2} = \lambda(\phi_{j-1/2,L}^{n+1/2})$ and $\lambda_j^n = \lambda(\Phi_j^n)$. They might be positive as well as negative. The maximum of the two is denoted by $\lambda_{\max}$. The first value $\phi_{1/2,L}^{n+1/2}$ is given by the left-hand boundary condition.

(ii) Compute the corresponding Courant number for the left state of the Riemann problem: $Cr_j = \lambda_{\max}\Delta t/\Delta x_j$.

(iii) Compute the left state of the Riemann problem at the interface using the following equations:

$$\phi_{j+1/2,L}^{n+1/2} = \Phi_j^n/Cr_j + (1 - Cr_j)\phi_{j-1/2,L}^{n+1/2} \quad \text{if } Cr_j \geqslant 1 \tag{2.16a}$$

$$\phi_{j+1/2,L}^{n+1/2} = \Phi_j^n \quad \text{if } Cr_j < 1 \tag{2.16b}$$

The second step consists of determining the right states of the Riemann problems. The computational domain is swept from right to left (decreasing j), starting from the right-hand boundary.

(iv) For each interface $j+1/2$, determine the wave speeds $\lambda_{j+3/2}^{n+1/2} = \lambda(\phi_{j+3/2,R}^{n+1/2})$ and $\lambda_{j+1}^n = \lambda(\Phi_{j+1}^n)$. They might be positive as well as negative. The minimum of the two is denoted by $\lambda_{\min}$. The value $\phi_{N+1/2,R}^{n+1/2}$ at the right-hand boundary $N+1/2$ is given by the boundary condition.

(v) Compute the corresponding Courant number for the right state of the Riemann problem: $Cr_{j+1} = -\lambda_{inx}\Delta t/\Delta x_{j+1}$

(vi) Compute the left state of the Riemann problem at the interface using the following equations:

$$\phi_{j+1/2,R}^{n+1/2} = \Phi_{j+1}^n/Cr_{j+1} + (1 - Cr_{j+1})\phi_{j+3/2,R}^{n+1/2} \quad \text{if } Cr_{j+1} \geqslant 1 \tag{2.17a}$$

$$\phi_{j+1/2,R}^{n+1/2} = \Phi_{j+1}^n \quad \text{if } Cr_{j+1} < 1 \tag{2.17b}$$

The third step is the solution of the Riemann problem at the cell interfaces. The left state of the Riemann problem at the cell interface $j+1/2$ is given by $\phi^{n+1/2}_{j+1/2,L}$ while the right state is given by $\phi^{n+1/2}_{j+1/2,R}$. Any standard Riemann solver can be used for this purpose. The fluxes at the cells interfaces are determined from the solution of the Riemann problems and used in Equation (2.2) to compute the balance over the computational cells and advance to the next time step.

3. 2×2 SYSTEMS OF NON-LINEAR CONSERVATION LAWS

3.1. *Inner cells*

The system of conservation laws that describes low-void ratio pipe transients is considered here. When the amount of gas in the pipe is small, it is possible to describe the two-phase system with a single fluid [10, 11]. This model is called the 'single component approximation'. In the absence of friction, the equations to be solved are the following:

$$\frac{\partial \boldsymbol{\phi}}{\partial t}+\frac{\partial \mathbf{F}}{\partial x}=0 \tag{3.1a}$$

$$\boldsymbol{\phi}=\begin{bmatrix}\mu\\ q\end{bmatrix},\quad \mathbf{F}=\begin{bmatrix}q\\ Ap+q^2/\mu\end{bmatrix} \tag{3.1b}$$

$$\frac{d}{d\mu}(Ap)=c^2=\frac{c_w^2}{1+\theta/p^{1+1/\alpha}} \tag{3.1c}$$

$$\theta=\eta_0\rho_0 c_w^2 p_0^{1/\alpha} \tag{3.1d}$$

$$p\eta^\alpha=p_0\eta_0^\alpha \tag{3.1e}$$

$$\rho_g\eta=\rho_{g,0}\eta_0 \tag{3.1f}$$

where A (m^2) is the pipe cross-sectional area, c (m s^{-1}) is the local speed of sound in the mixture, c_w (m s^{-1}) is the local speed of sound in the absence of gas, p (Pa) is the pressure, p_0 (Pa) is a reference pressure, q (kg s^{-1}) is the mass discharge, α (dimensionless) is a coefficient characterizing the behaviour of the gas fraction, η (dimensionless) is the fraction of volume occupied by the gas phase, η_0 (dimensionless) is the value of η for the reference pressure p_0, μ (kg m^{-1}) is the mass per unit length of pipe, ρ_g (kg m^{-3}) is the fluid density and $\rho_{g,0}$ (kg m^{-3}) is the fluid density at pressure p_0. Equations (3.1c,d) for the celerity are a generalization [12] of a formula provided by other authors [10, 13] under the assumption of no slip between the gas and the liquid phases. Isothermal and adiabatic gas behaviours can be obtained by setting α equal to 1 and 1.4 respectively. Equation (3.1a) can be rewritten in the classical non-conservative form:

$$\frac{\partial \boldsymbol{\phi}}{\partial t}+\mathbf{J}\frac{\partial \boldsymbol{\phi}}{\partial x}=0 \tag{3.2a}$$

$$\mathbf{J}=\begin{bmatrix}0 & 1\\ c^2-u^2 & 2u\end{bmatrix} \tag{3.2b}$$

The eigenvalues λ_k and eigenvectors $\mathbf{e}^{(k)}$ of $\mathbf{J}$ are well known:

$$\lambda_k = u + (-1)^k c \quad k = 1,2 \tag{3.3a}$$

$$\mathbf{e}^{(k)} = \begin{bmatrix} 1 \\ \lambda_k \end{bmatrix} \quad k = 1,2 \tag{3.3b}$$

Although the celerity is highly dependent on the pressure p and may drop down to extremely low values, the conditions under which pipe systems are operated are such that the fluid velocity u is in general not higher than a few m s^{-1}. For this reason, it is extremely unusual to find supercritical conditions. Most of the time, the eigenvalues of the 2×2 system have opposite signs. The sequel focuses on subcritical flow.

The flux at interface $(j + 1/2)$ is obtained from the solution of a Riemann problem at the interface:

$$\phi(x) = \phi_{j+1/2,L} \quad \text{for } x \leqslant x_{j+1/2} \tag{3.4a}$$

$$\phi(x) = \phi_{j+1/2,R} \quad \text{for } x > x_{j+1/2} \tag{3.4b}$$

The key of the algorithm lies in the estimate of $\phi_{j+1/2,L}$ and $\phi_{j+1/2,R}$. By definition (see Reference [11] and Appendix B), the following relationships are valid (see Figure 4):

$$\phi_{j+1/2,L} = \frac{1}{\Delta t} \int_I^B \phi^-_{j+1/2}(t)\mathrm{d}t \tag{3.5a}$$

$$\phi_{j+1/2,R} = \frac{1}{\Delta t} \int_I^B \phi^+_{j+1/2}(t)\mathrm{d}t \tag{3.5b}$$

where $\phi^-_{j+1/2}(t) = Lim_{\varepsilon\to 0^-}\ \phi(x = x_{j+1/2} + \varepsilon, t)$ and $\phi^+_{j+1/2}(t) = Lim_{\varepsilon\to 0^+}\ \phi(x = x_{j+1/2} + \varepsilon, t)$. Consider $\phi_{j+1/2,L}$ alone. The integral in Equation (3.5a) can be separated into two parts:

$$\phi_{j+1/2,L} = \frac{1}{\Delta t} \int_I^L \phi^-_{j+1/2}(t)\,\mathrm{d}t + \frac{1}{\Delta t} \int_L^B \phi^-_{j+1/2}(t)\,\mathrm{d}t \tag{3.6}$$

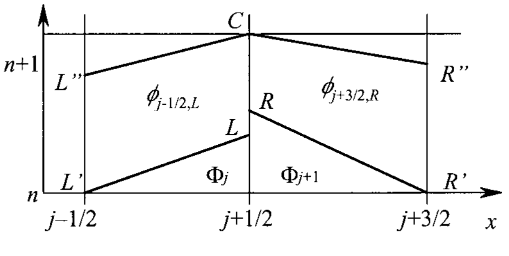

Figure 4. Sketch of the method for a 2×2 system of equations.

where L is the intersection of the characteristic passing at $(j-1/2, n)$ and interface $j+1/2$ in the (x,t) plane. The first integral on the right-hand side of Equation (3.6) can be approximated by:

$$\frac{1}{\Delta t}\int_I^L \phi_{j+1/2}^-(t)\,\mathrm{d}t \cong \frac{\tau_L}{\Delta t}\frac{1}{\Delta x_j}\int_I^{L'} \phi^n(x)\,\mathrm{d}x = \Phi_j^n \tag{3.7}$$

where τ_L is the time corresponding to the location of L on the time axis. The second integral is evaluated as:

$$\frac{1}{\Delta t}\int_L^B \phi_{j+1/2}^-(t)\,\mathrm{d}t = \frac{\Delta t - \tau_L}{\Delta t}\frac{1}{\tau_{L''} - \tau_{L'}}\int_{L'}^{L''} \phi_{j-1/2}^-(t)\,\mathrm{d}t \tag{3.8}$$

where τ_L' and τ_L'' are the times corresponding to the locations of L' and L'' on the time axis respectively. Assuming once again that $\phi_{j-1/2}^-(t)$ is constant, this reduces to:

$$\frac{1}{\Delta t}\int_{L'}^{L''} \phi_{j+1/2}^-(t)\,\mathrm{d}t = \frac{\Delta t - \tau_L}{\Delta t}\phi_{j-1/2,L}^{n+1/2} \tag{3.9}$$

The only task left is the estimate of the time τ_L. As explained in Section 2.2, in order to avoid oscillations and possible instabilities, it is chosen to overestimate the slope of the characteristic issuing from A'. τ_L is then given by:

$$\tau_L = \frac{\Delta x_{j-1}}{\max(\lambda_{2,j}^n, \lambda_{2,j-1/2,L})} \tag{3.10a}$$

$$\lambda_{2,j}^n = u_j^n + c_j^n \tag{3.10b}$$

$$\lambda_{2,j-1/2,L}^n = u_{j-1/2,L} + c_{j-1/2,L} \tag{3.10c}$$

where u_j^n and c_j^n are the velocity and local speed of sound over cell j at time level n and $u_{j+1/2,L}$ and $c_{j+1/2,L}$ are the velocity and local speed of sound derived from the left state of the Riemann problem at the interface $j+1/2$. Finally, Equation (3.6) becomes:

$$\phi_{j+1/2,L} = \frac{\tau_L}{\Delta t}\Phi_j^n + \left(1 - \frac{\tau_L}{\Delta t}\right)\phi_{j-1/2,L} \tag{3.11}$$

A similar reasoning for the right state of the Riemann problem yields:

$$\phi_{j+1/2,R} = \frac{\tau_R}{\Delta t}\Phi_{j+1}^n + \left(1 - \frac{\tau_R}{\Delta t}\right)\phi_{j+3/2,R} \tag{3.12}$$

where τ_R is given by:

$$\tau_R = -\frac{\Delta x_j}{\min(\lambda_{1,j+1}^n, \lambda_{1,j+3/2,R})} \tag{3.13a}$$

$$\lambda_{1,j+1}^n = u_{j+1}^n - c_{j+1}^n \tag{3.13b}$$

$$\lambda_{1,j+3/2,R}^n = u_{j+3/2,R} - c_{j+3/2,R} \tag{3.13c}$$

Once $\boldsymbol{\phi}_{j+1/2,L}$ and $\boldsymbol{\phi}_{j+1/2,R}$ are known, the Riemann problem can be solved using standard techniques. The solver that was retained is an approximate-state solver, based on the assumption of two rarefaction waves. The values $\mu_{j+1/2}^{n+1/2}$ and $q_{j+1/2}^{n+1/2}$ of μ and q at the interface are found by solving the following differential relationships [11, 12]:

$$q_{j+1/2}^{n+1/2} - q_{j+1/2,L}^{n+1/2} = \frac{1}{2}(u_{j+1/2}^{n+1/2} - c_{j+1/2}^{n+1/2} + u_{j+1/2,L} - c_{j+1/2,L})(\mu_{j+1/2}^{n+1/2} - \mu_{j+1/2,L}^{n+1/2}) \tag{3.14a}$$

$$q_{j+1/2}^{n+1/2} - q_{j+1/2,R}^{n+1/2} = \frac{1}{2}(u_{j+1/2}^{n+1/2} + c_{j+1/2}^{n+1/2} + u_{j+1/2,R} + c_{j+1/2,R})(\mu_{j+1/2}^{n+1/2} - \mu_{j+1/2,R}^{n+1/2}) \tag{3.14b}$$

Once $\boldsymbol{\phi}_{j-1/2}^{n+1/2}$ and $\boldsymbol{\phi}_{j+1/2}^{n+1/2}$ are known, the numerical solution can be advanced in time using the classical formula:

$$\Phi_j^{n+1} = \Phi_j^n + \frac{\Delta t}{\Delta x_j}[\mathbf{F}(\boldsymbol{\phi}_{j-1/2}^{n+1/2}) - \mathbf{F}(\boldsymbol{\phi}_{j+1/2}^{n+1/2})] \tag{3.15}$$

Note that the assumption of two rarefaction waves for the Riemann solver is made *a priori*, regardless of the real wave pattern present in the solution. This assumption is not checked *a posteriori*, but theoretical considerations [14] as well as numerical experiments [10, 13] show that this assumption yields a fairly good approximation of the variable within the region of intermediate state, even if shock waves are present in the solution.

3.2. Boundary conditions

Equations (3.11) and (3.12) form two sets of N recurrence relationships. Provided that $\boldsymbol{\phi}_{1/2,L}$ is known (average value of $\boldsymbol{\phi}$ at the left-hand boundary of the computational domain), the values $\boldsymbol{\phi}_{j-1/2,L}$ can be determined by performing a single sweep along increasing j. Similarly, provided that $\boldsymbol{\phi}_{N+1/2,R}$ is known at the right-hand boundary of the computational domain (N being the number of computational cells in the domain) $\boldsymbol{\phi}_{j-1/2,R}$ can be calculated by performing a sweep along decreasing j. The sequel explains how to determine the values $\boldsymbol{\phi}_{1/2,L}$ and $\boldsymbol{\phi}_{N+1/2,R}$.

Consider the left-hand boundary. It was shown in a previous publication [12] that the following conditions must be satisfied at the boundary:

$$q_B - q_{1/2,R} = \tfrac{1}{2}(u_B + c_B + u_{1/2,R} + c_{1/2,R})(\mu_B - \mu_{1/2,R}) \tag{3.15a}$$

$$f_B(\mu_B, q_B) = 0 \tag{3.15b}$$

where q_B and μ_B are the (unknown) average values of q and μ at the boundary between time levels n and $n+1$. f_B is a function that reflects the nature of the boundary (e.g. prescribed discharge, prescribed pressure, relationship between pressure and discharge, etc.). As there are $N+1$ interfaces in the system, there are $2N+2$ unknowns $q_{j+1/2}, \mu_{j+1/2}$. These unknowns are related by $N-1$ equations of the form of Equation (3.11) and N equations of the form of Equation (3.12) for the inner interfaces, and two sets of equations of the form of Equation (3.15a, b) for the boundaries. Since the number of equations matches the number of unknowns, the problem can be solved. The system of equations is 4-diagonal and can be solved easily using a classical double-sweep algorithm [15]. A much easier solution consists of sweeping the domain twice in each direction, so that boundary conditions are correctly accounted for. Experience shows that more iterations are in general not needed.

There is a case where the inversion of a system is not needed: if the time step and the sizes of at least one cell m in the computational domain are such that the Courant number in this cell is lower than unity, the following procedure can be followed.

(i) Average the reconstructed profile of the variable at time level n over the domain of dependence of the second characteristic issuing from interface $m+1/2$. It was shown in an earlier work [16] that this average value can be taken as an approximation for $\phi_{m+1/2,L}$.
(ii) Use Equation (3.11) to determine the values $\phi_{j+1/2,L}$ for ascending j.
(iii) Average the reconstructed profile of the variable at time level n over the domain of dependence of the first characteristic issuing from interface $N+1/2$. This average value gives $\phi_{N+1/2,R}$.
(iv) Use Equation (3.12) to determine the values $\phi_{j+1/2,R}$ for descending j.

A similar sequence can be repeated for the cells located to the left of cell m. The sequence of operations (i)–(iv) is no more time-consuming than classical explicit techniques. The values at the boundaries can be determined using a standard iterative technique. In References [11] and [12], the Newton–Raphson method was used.

3.3. Courant numbers smaller than unity

As shown in Appendix A, time-line interpolation is stable only for Courant numbers greater than unity. In cells where it is lower than 1, a classical explicit formulation must be used. Application of the DPM technique to reconstruction of profiles in space has been demonstrated in an earlier publication [11]. $\phi_{j+1/2,L}$ can be approximated with a reasonable precision by the average of the reconstructed profile over the domain of dependence of the characteristic heading to the right (see Appendix B). Conversely, $\phi_{j+1/2,R}$ can be taken equal to the average of the reconstructed profile over the domain of dependence of the characteristic heading to the left.

4. COMPUTATIONAL EXAMPLES

4.1. Scalar equations

The proposed method was applied to the scalar linear advection equation and to the inviscid Burger's equation. For the linear advection equation, the advection velocity was set equal to 1 m s^{-1} everywhere, with a time step $\Delta t = 1$ s. The cell size was taken equal to $Dx = 1$ m everywhere, except between $x = 10$ m and 15 m, where it was taken equal to 0.2 m. Consequently, the Courant number is equal to 5 between $x = 10$ and $x = 15$ and to unity everywhere else. Figure 5 shows the simulation results for an initially square profile of width 10 m after 20 computational time steps. In order to facilitate comparison with standard methods, the numerical solution obtained using the time-line interpolation is compared to that given by the classical first-order upwind implicit scheme. It can be seen that the proposed approach leads to much less numerical diffusion and less phase error than the standard implicit approach.

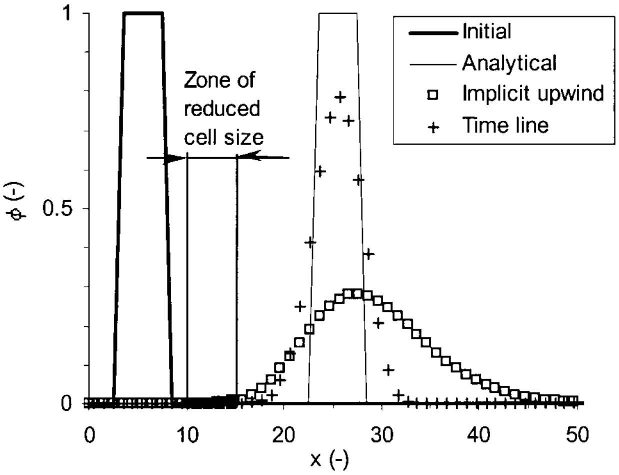

Figure 5. Solution of the linear advection equation after 20 s over an irregular mesh using the first-order implicit (upwind) scheme and the time-line interpolation scheme. The Courant number is equal to 5 between $x = 10$ and $x = 15$, and equal to 1 everywhere else.

The method was applied to the solution of the inviscid Burgers equation over a regular mesh for an initially square profile. The cell size was taken equal to 1 m everywhere, the computational time step was taken equal to 0.5 s. The minimum value of ϕ was $1\,\mathrm{m\,s^{-1}}$ and its maximum value was $2\,\mathrm{m\,s^{-1}}$, therefore the Courant number is comprised of between 1 and 2 in the present simulation. The behaviour of the analytical solution is well known: the front of the profile is a shock and its tail degenerates into a rarefaction wave. It is easy to check that at $t = 10$ s, the head of the rarefaction wave catches up the shock wave and that the resulting profile is triangular. Figure 6 shows the analytical solution at $t = 10$s and the computed profiles obtained using the proposed time-line interpolation method and the classical first-order implicit upwind scheme. As in the linear case, the first-order upwind scheme introduces a stronger diffusion and a larger phase error than the time-line interpolation.

4.2. 2 × 2 *system of conservation laws for two-phase flow in pipes*

The system of Equation (3.1) was solved to simulate the flow resulting from a sudden pressure drop at the extremity of a pipe (see Reference [12] for more details on this test case). At the beginning of the simulation, the fluid is assumed to be at rest. The pressure drop is assumed to occur instantaneously at the left-hand end of the pipe. At the right-hand end of the pipe, the pressure is kept equal to its initial value.

The fluid and pipe properties can be found in Table I. Table II summarizes the initial and boundary conditions.

A first calculation was carried out over a period of 80 s using the classical explicit Godunov scheme [12] for a uniform cell size $\Delta x = 100$ m. The time step was limited so that the maximum Courant number over all cells was equal to unity. A second calculation was carried using an irregular discretization: between $x = 1400$ m and $x = 1600$ m, the 14th and 16th cells, of equal length $\Delta x_{14} = \Delta x_{16} = 99.5$ m were separated by a cell of length $\Delta x_{15} = 1$ m. All

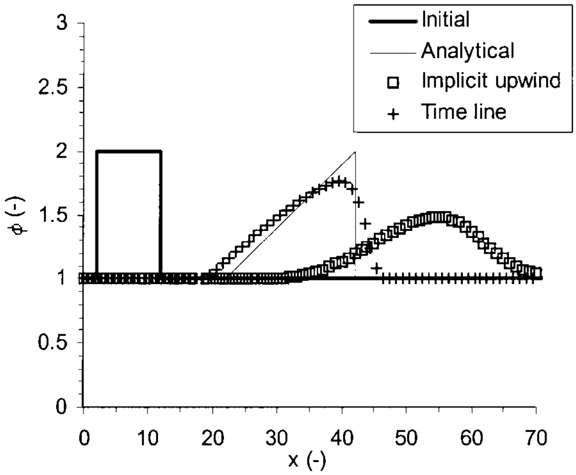

Figure 6. Solution of the inviscid Burger's equation after 10 s using the first-order implicit (upwind) scheme and the time-line interpolation scheme. The Courant number is comprised between 1 and 2.

Table I. Physical parameters for test case 1.

Parameter	Symbol and unit	Value
Pipe length	L (m)	3000
Nominal cross-sectional area	A_0 (m^2)	0.29
Nominal celerity	c_0 (m s^{-1})	981.4
Nominal density	ρ_0 (kg m^{-3})	992
Coefficient in the perfect gas equation	α (—)	1
Reference mass per unit length	μ_0 (kg m^{-1})	289.9
Reference void fraction	$\eta_{g,0}$ (—)	2×10^{-3}
Reference pressure	p_0 (Pa)	101 325

Table II. Initial and boundary conditions for the test case.

Parameter	Symbol and unit	Value
Initial mass discharge	q_i (kg s^{-1})	0
Initial pressure	P_i (Pa)	5×10^5
Pressure at the left end of the pipe	p_{LE} (Pa)	10^5
Pressure at the right end of the pipe	p_{RE} (Pa)	5×10^5

other cells remained unchanged. No time-line interpolation was used and the time step Δt was therefore chosen such that the maximum Courant number in cell 15 of width $\Delta x = 1$ m was equal to unity. This leads to a maximum Courant number of about 10^{-2} in the other cells. A third calculation was carried out on the same grid using the time-line interpolation technique. The time step was taken equal to that of the first calculation. A maximum Courant number of 100 was therefore achieved in cell 15. Note that, owing to stability constraints, the computational time step in the second calculation was 100 times smaller than it was in the first and third simulations.

Figure 7 shows the computed pressure profiles at various times for the three calculations. Figure 7(a) shows the computational results for a uniform cell size, Figure 7(b) shows the results obtained with the irregular grid without time-line interpolation and Figure 7(c) shows the calculation results on the irregular grid with time-line interpolation. It can be seen that, when the explicit formulation is used, the time step reduction induces a strong damping of the computed profile (Figure 7(b)). This is particularly visible in cell 15, where the profile is almost flat. Profile damping can also be observed quite clearly on the tail of the rarefaction wave heading to the right at time $t = 2\,\mathrm{s}$. The time-line interpolation eliminates these problems to a large extent.

Figure 8 shows the pressure history recorded at the middle of the pipe for the three calculations. In the first calculation, $x = 1500\,\mathrm{m}$ corresponds to the interface between cells 14 and 15. The value of the pressure at the interface was computed by averaging the values of the pressure in these cells. In the second and third calculations, $x = 1500\,\mathrm{m}$ corresponds to the centre of cell 15 and therefore no averaging was needed. The figure confirms the strong damping introduced by the time step limitation in the second simulation. The time-line interpolation technique, which allows bigger time steps to be used, was seen to produce no noticeable difference with the simulation carried out on the regular grid.

5. CONCLUSIONS

The time-line interpolation technique uses the theory of characteristics to provide an equivalence between the space- and time-dimensions of the domain of dependence of the numerical solution. This equivalence allows computational grids to be designed in such a way that calculations can be carried out without leading to numerical instability. Besides the equivalence between the time and space extents of the domain of dependence, the key point in the stabilization of the scheme is the overestimation of propagation celerity. This allows oscillations in the computed profiles to be eliminated. Time-line interpolation allows simulations to be carried out at Courant number values greater than unity. The implementation of this method for the simulation of low-void ratio pipe transients proves to be successful and to increase the accuracy of the numerical solution considerably, especially when local grid refinement is needed. Ongoing research focuses on the design of higher-order time-line interpolation techniques.

APPENDIX A: LINEAR STABILITY ANALYSIS

A.1. Consistency analysis

Consider linear scalar advection, where the flux is given by Equation (2.2a). In this case, the recurrence relationship for the flux at the cell interfaces is given by Equation (2.10):

$$F_{j+1/2} = \frac{a}{Cr_j}\Phi_j^n + \left(1 - \frac{1}{Cr_j}\right)F_{j-1/2} \tag{2.10}$$

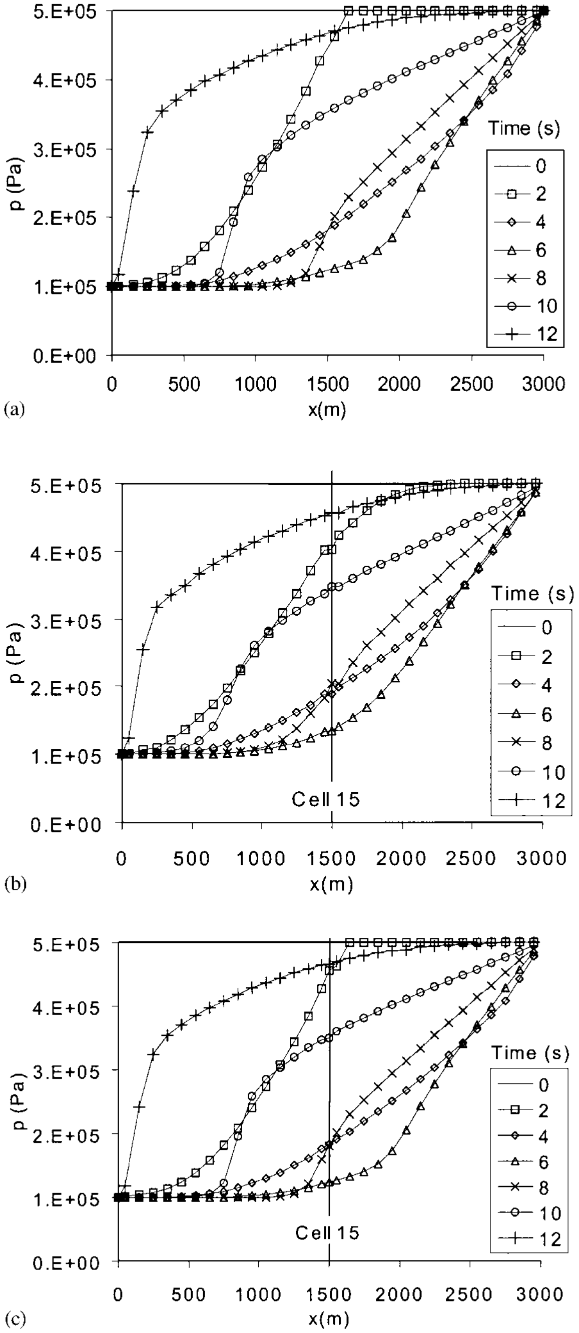

Figure 7. Computed pressure profiles at various dates using the DPM scheme without grid refinement (a), with grid refinement without time-line interpolation (b), and with grid refinement and time-line interpolation (c).

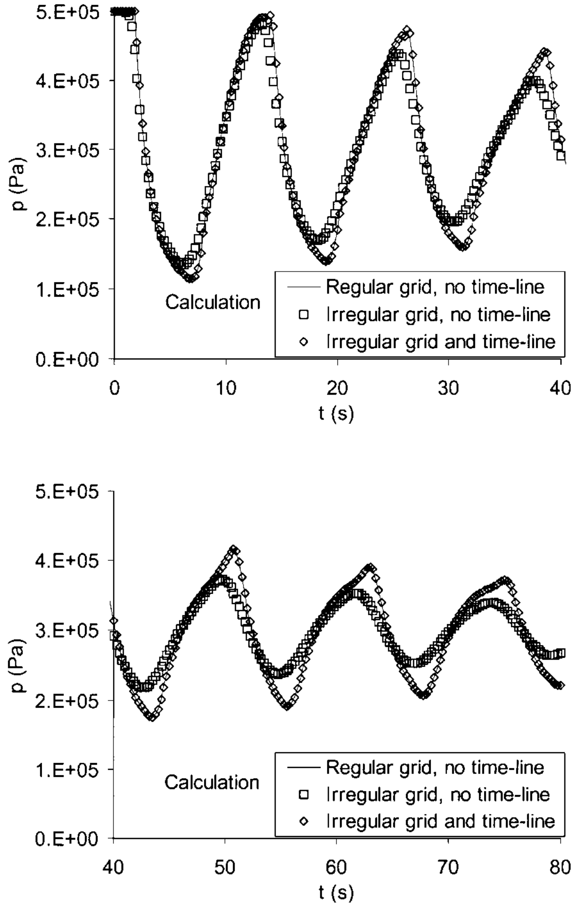

Figure 8. Pressure history at the middle of the pipe using a regular grid and an irregular one, with and without time-line interpolation.

Substituting Equation (2.10) into Equation (2.2) yields:

$$\Phi_j^{n+1}=\Phi_j^n+\frac{\Delta t}{\Delta x_j}\left[F_{j-1/2}^{n+1/2}-\frac{a}{Cr}\Phi_j^n-\left(1-\frac{1}{Cr_j}\right)F_{j-1/2}^{n+1/2}\right] \tag{A1}$$

This can be simplified into:

$$F_{j-1/2}=a\Phi_j^{n+1} \tag{A2}$$

The scheme of Equation (2.2) can finally be rewritten as:

$$\Phi_j^{n+1}=\Phi_j^n+Cr_j(\Phi_j^{n+1}-\Phi_{j+1}^{n+1}) \tag{A3}$$

which is a first-order, implicit formulation. The truncation error associated to this formulation is given by:

$$TE = \frac{\Delta t^2}{2}\frac{\partial^2 \phi}{\partial t^2} - Cr\frac{\Delta x^2}{2}\frac{\partial^2 \phi}{\partial x^2} + \text{HOT} \tag{A4}$$

Using the classical relationship, obtained from the discretization:

$$\frac{\partial^2 \phi}{\partial t^2} = a^2\frac{\partial^2 \phi}{\partial x^2} + \text{HOT} \tag{A5}$$

Equation (A4) can be rewritten as:

$$TE = \frac{\Delta x^2}{2}(Cr^2 - Cr)\frac{\partial^2 \phi}{\partial x^2} + \text{HOT} \tag{A6}$$

The proposed formulation also introduces a positive diffusion coefficient in the truncation error when the Courant number is strictly greater than unity. The algorithm is then first-order accurate and stable for Courant numbers greater than unity. Note that it is different from the classical implicit formulation that uses:

$$F_{j-1/2} = a\Phi_{j-1}^{n+1} \tag{A7}$$

and for which the truncation error is:

$$TE = \frac{\Delta x^2}{2}(Cr^2 + Cr)\frac{\partial^2 \phi}{\partial x^2} + \text{HOT} \tag{A8}$$

A.2. Stability analysis

The stability analysis consists of seeking the solution to Equation (A3) in the form:

$$\Phi_j^n = K\exp(i\lambda_r n\Delta t - \lambda_i n\Delta t)\exp(i\mu j\Delta x) \tag{A9}$$

where K, λ_i, λ_r and μ are real constants. Assuming that the Courant number is constant and equal to Cr, substituting Equation (A9) into Equation (A3) yields:

$$A_N = 1 + Cr[A_N - A_N\exp(i\mu\Delta x)] \tag{A10a}$$

$$A_N = \exp(i\lambda_r\Delta t - \lambda_i\Delta t) \tag{A10b}$$

where A_N is called the numerical amplification factor. Equation (A10a) yields directly the expression for A_N:

$$A_N = \frac{1}{z} \tag{A11a}$$

$$z = 1 + Cr[\exp(i\mu\Delta x) - 1] \tag{A11b}$$

The modulus of the numerical amplification factor is the inverse of the modulus of z. Figure A1 gives a graphical representation of the location of z in the complex plane. z is located on a circle of radius Cr, the centre of which is located at $1 - Cr$. For $Cr \geqslant 1$, z is

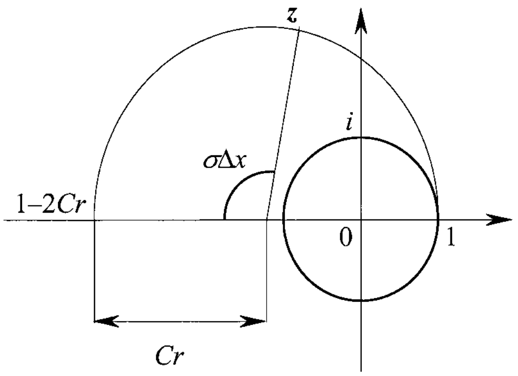

Figure A1. Time-line interpolation: graphical interpretation for the numerical amplification factor. The complex number z is the inverse of A_N.

located outside or on the unit circle in the complex plan. Consequently, $|z| \geqslant 1$, hence $|A_N| \leqslant 1$. The discretization is always stable for $Cr \geqslant 1$. In addition to the numerical amplification factor, the global amplification factor A_G gives useful information on the behaviour of the scheme [13]. It is defined as follows:

$$A_G = A_N^{1/Cr} \tag{A12}$$

which represents the factor by which a wave of given length is amplified over a fixed amount of time, whereas the numerical amplification factor represents the amount by which the wave is amplified over one time step. For practical purposes, the information provided by the global amplification factor is more useful than that provided by the numerical amplification factor, because the length of the simulation is the interesting quantity to modellers.

The numerical celerity convergence factor c_N is given by:

$$c_N = -\frac{\lambda_r}{a\mu} = -\frac{\mathrm{Arg}(A_N)}{a\mu\Delta t} = -\frac{\mathrm{Arg}(A_N)}{Cr\mu\Delta x} = \frac{\mathrm{Arg}(z)}{Cr\mu\Delta x} \tag{A13}$$

The argument of z can be deduced easily from Equation (A11b):

$$\mathrm{Arg}(z) = \mathrm{Arc}\tan\left[\frac{Cr\sin(\mu\Delta x)}{1 - Cr + \cos(\mu\Delta x)}\right] \tag{A14}$$

Substituting Equations (A8) and (A7) into Equation (A6) yields:

$$c_N = \frac{\mathrm{Arc}\tan\left[\dfrac{Cr\sin(\mu\Delta x)}{1 - Cr + Cr\cos(\mu\Delta x)}\right]}{Cr\mu\Delta x} \tag{A15}$$

Figure A2 display the amplitude and phase portraits for the present discretization. A_N, A_G and c_N are given as functions of the wave number $M = 2\pi/(\mu\Delta x)$. It can be seen in particular that the extremely diffusive behaviour of the scheme at high Courant numbers is compensated for since, owing to the larger time step, the computations have to be repeated fewer times than for small values of the Courant number. Figure A2(b) also shows that the uniform time-line

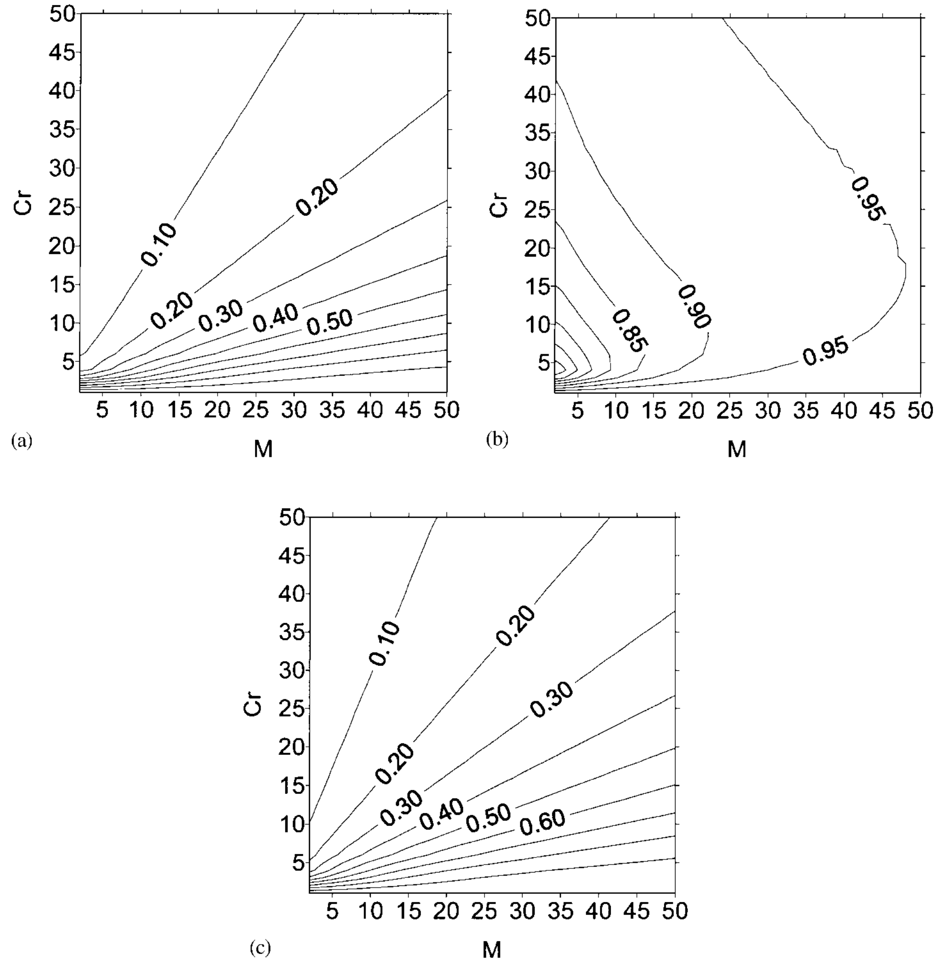

Figure A2. Amplitude and phase portraits for the uniform time-line interpolation. Numerical (a) and global (b) amplification factor, celerity convergence factor (c). The wave number M is defined as $M = 2\pi/(\sigma\Delta x)$. The spacing of the contour lines for the global amplification factor (b) is 0.05.

interpolation exhibits minimum performance for intermediate values of the Courant number (between 2 and 40).

APPENDIX B: PROFILE AVERAGING FOR THE RIEMANN PROBLEM

The considerations presented in the present Appendix have already been developed in a previous publication [6]. They are presented here for the sake of clarity only.

Consider first the case where the Courant number is lower than unity, that is where the time step is too small for the characteristics to cross the cell. Assume that the initial profile of ϕ (obtained from a reconstruction) is known at time level n. At the interface between two computational cells, this reconstructed profile is used to define the Riemann problem by averaging the eigenvectors over their domain of dependence. The flux at the interface is given by:

$$\mathbf{F}_{j+1/2} = \mathbf{F}(\phi_{j+1/2}) = \mathbf{F}(\mathbf{K}\boldsymbol{\sigma}_{j+1/2}) \tag{B1a}$$

$$\mathbf{K} = \begin{bmatrix} 1 & \mathbf{1} \\ \lambda_1 & \lambda_2 \end{bmatrix} \tag{B1b}$$

$$\lambda_k = q/\mu + (-1)^k c \tag{B1c}$$

where $\mathbf{K}$ is the matrix formed by the eigenvectors of the Jacobian matrix $\mathbf{J} = \partial\mathbf{F}/\partial\boldsymbol{\phi}$ (see Section 3), λ_k, $k = 1,2$ are the eigenvalues of $\mathbf{J}$, and $\boldsymbol{\sigma} = \mathbf{K}^{-1}\boldsymbol{\phi}$ contains the coordinates of $\boldsymbol{\phi}$ in the base of the eigenvectors. In the case of a Riemann problem, i.e. with constant right and left states, $\boldsymbol{\sigma}_{j+1/2}$ is a constant. But in general, the reconstructed profile is not constant over space. This type of problem is referred to as a generalized Riemann problem. In that case, the value of $\boldsymbol{\sigma}_{j+1/2}$ depends on time. We are therefore interested in the average $\mathbf{F}_{j+1/2}$ of the flux $\mathbf{F}_{j+1/2}$ over time:

$$\bar{\mathbf{F}}_{j+1/2} = \frac{1}{\Delta t}\int_0^{\Delta t} \mathbf{F}_{j+1/2}(t)\,\mathrm{d}t \tag{B2}$$

To estimate this value, a linearization is applied to approximate $\bar{\mathbf{F}}_{j+1/2}$ with:

$$\bar{\mathbf{F}}_{j+1/2} = \mathbf{F}(\mathbf{K}\bar{\boldsymbol{\sigma}}_{j+1/2}) \tag{B3a}$$

$$\bar{\sigma}_{j+1/2} = \frac{1}{\Delta t}\int_0^{\Delta t} \boldsymbol{\sigma}_{j+1/2}(t)\,\mathrm{d}t \tag{B3b}$$

The kth component $\bar{\boldsymbol{\sigma}}^{(k)}_{j+1/2}$ of $\bar{\boldsymbol{\sigma}}_{j+1/2}$ is given by:

$$\bar{\boldsymbol{\sigma}}^{(k)}_{j+1/2} = \frac{1}{\Delta t}\int_0^{\Delta t} \boldsymbol{\sigma}^{(k)}_{j+1/2}(t)\,\mathrm{d}t = \frac{1}{\zeta_k}\int_{x_{p+1/2}-\zeta_k}^{x_{j+1/2}} \boldsymbol{\sigma}^{(k)}_j(x)\,\mathrm{d}x \tag{B4}$$

where $\zeta_k = \lambda_k \Delta t$ is the horizontal distance covered by the kth characteristic during time Δt (also called the domain of dependence associated to the kth characteristic). Index p denotes the cell in which the foot of the characteristic is located.

Assume that $p = j$. If both λ_1 and λ_2 are positive in cell j (supercritical flow), then both components of $\bar{\boldsymbol{\sigma}}_j$ are fully determined in cell j, because both domains of dependence of the interface $j + 1/2$ lie in cell j. The left state $\boldsymbol{\phi}_{j+1/2,L}$ is then deduced from:

$$\boldsymbol{\phi}_{j+1/2,L} = \mathbf{K}\bar{\boldsymbol{\sigma}}_j \tag{B5}$$

Pipe transients are characterized by subcritical flows. In that case, the foot of the second characteristic only lies in cell j, whereas the first one has its foot in cell $j+1$. Consequently, the value of the first component $\bar{\boldsymbol{\sigma}}^{(1)}_j$ of $\bar{\boldsymbol{\sigma}}_j$ does not have any influence on the solution of the Riemann problem at interface $j + 1/2$. Then the same relationship can be used for both $\bar{\boldsymbol{\sigma}}^{(1)}_{j+1/2}$

and $\bar{\boldsymbol{\sigma}}_{j+1/2}^{(2)}$:

$$\bar{\boldsymbol{\sigma}}_j^{(k)} = \frac{1}{\zeta_2}\int_{x_{j+1/2}-\zeta_2}^{x_{j+1/2}} \boldsymbol{\sigma}_j^{(k)}(x)\,\mathrm{d}x, \quad k=1,2 \tag{B6}$$

If matrix **K** is assumed to be constant over the integration interval, substituting Equation (B5) into Equation (B6) gives:

$$\boldsymbol{\phi}_{j+1/2,L} = \frac{1}{\zeta_2}\int_{x_{j+1/2}-\zeta_2}^{x_{j+1/2}} \boldsymbol{\phi}_j(x)\,\mathrm{d}x \tag{B7}$$

A similar reasoning gives the formula for the right state of the Riemann problem:

$$\boldsymbol{\phi}_{j+1/2,R} = \frac{1}{\zeta_1}\int_{x_{j+1/2}-\zeta_1}^{x_{j+1/2}} \boldsymbol{\phi}_{j+1}(x)\,\mathrm{d}x \tag{B8}$$

Therefore, in the subcritical case, the left and right states of the Riemann problem can be obtained by simply averaging the reconstructed profile over the domain of dependence of the characteristics.

ACKNOWLEDGEMENTS

The author would like to thank Profs J. A. Cunge and M. J. Hall from IHE for their comments and suggestions, as well as for checking the english of the present contribution.

REFERENCES

1. Fryxell BA, Woodward PR, Colella P, Winckler KH. An implicit–explicit hybrid method for Lagrangian hydrodynamics. *Journal of Computational Physics* 1986; **63**:283–310.
2. Collins JP, Colella P, Glaz HM. An implicit–explicit Eulerian Godunov scheme for compressible flow. *Journal of Computational Physics* 1995; **116**:195–211.
3. Dai W, Woodward PR. Iterative implementation of an implicit–explicit hybrid scheme for hydrodynamics. *Journal of Computational Physics* 1996; **124**(1):217–229.
4. Dai W, Woodward PR. A second-order iterative implicit–explicit hybrid scheme for hyperbolic systems of conservation laws. *Journal of Computational Physics* 1996; **128**(1):181–196.
5. LeVeque RJ. Large time step chock-capturing techniques for scalar conservation laws. *SIAM Journal of Numerical Analysis* 1982; **19**(6):1091–1109.
6. LeVeque RJ. Convergence of a large time step generalization of Godunov's method for conservation laws. *Communications in Pure and Applied Mathematics* 1984; **37**:463–477.
7. LeVeque RJ. High resolution finite volume methods on arbitrary grids via wave propagation. *Journal of Computational Physics* 1988; **78**:36–63.
8. Roe PL. Approximate Riemann solvers, parameter vectors and difference schemes. *Journal of Computational Physics* 1981; **43**:357–372.
9. Goldberg DE, Wylie EB. Characteristics method using time-line interpolations. *Journal of Hydrological Engineering ASCE* 1983; **109**(5):670–683.
10. Wylie EB. Simulation of vaporous and gaseous cavitation. *Journal of Fluids & Engineering*, *ASME* 1984; **106**:307–311.
11. Guinot V. The discontinuous profile method (DPM) for simulating two-phase flow in pipes using the single component approximation. *International Journal for Numerical Methods in Fluids*, accepted, for publication.
12. Guinot V. Numerical simulation of two-phase flow in pipes using Godunov Method. *International Journal for Numerical Methods in Engineering* 2000; **50**:1169–1189.
13. Wylie EB, Streeter VL. *Fluid Transients in Systems*. Prentice-Hall: Engelwood Cliffs, NJ, 1993.
14. Dukowicz JK. A general, non-iterative Riemann solver for Godunov's method. *Journal of Computational Physics* 1985; **61**:119–137.
15. Abbott MB, Minns AW. *Computational Hydraulics*. Ashgate, 1998.
16. Guinot V. Boundary condition treatment in 2 × 2 propagation systems. *International Journal for Numerical Methods in Engineering* 1998; **42**:647–666.